Commun. Comput. Phys.
doi: 10.4208/cicp.OA-2018-0034

Vol. **26**, No. 1, pp. 87-113
July 2019

Semi-Implicit Spectral Deferred Correction Method Based on the Invariant Energy Quadratization Approach for Phase Field Problems

Ruihan Guo[1] and Yan Xu[2,*]

[1] *School of Mathematics and Statistics, Zhengzhou University, Zhengzhou, Henan 450001, P.R. China.*
[2] *School of Mathematical Sciences, University of Science and Technology of China, Hefei, Anhui 230026, P.R. China.*

Received 5 February 2018; Accepted (in revised version) 24 July 2018

Abstract. This paper presents a high order time discretization method by combining the semi-implicit spectral deferred correction method with energy stable linear schemes to simulate a series of phase field problems. We start with the linear scheme, which is based on the invariant energy quadratization approach and is proved to be linear unconditionally energy stable. The scheme also takes advantage of avoiding nonlinear iteration and the restriction of time step to guarantee the nonlinear system uniquely solvable. Moreover, the scheme leads to linear algebraic system to solve at each iteration, and we employ the multigrid solver to solve it efficiently. Numerical results are given to illustrate that the combination of local discontinuous Galerkin (LDG) spatial discretization and the high order temporal scheme is a practical, accurate and efficient simulation tool when solving phase field problems. Namely, we can obtain high order accuracy in both time and space by solving some simple linear algebraic equations.

AMS subject classifications: 65M60, 35L75, 35G25

Key words: Phase field problems, local discontinuous Galerkin method, linear scheme, invariant energy quadratization approach, semi-implicit spectral deferred correction method.

1 Introduction

The phase field model has been used successfully for modeling a variety of interfacial phenomena like microstructure evolution [3] and the physics of phase transitions [16]. The key idea of phase field model is to replace the sharp interface by a thin transition lays, it takes two distinct values (for instance, $+1$ and -1) in each of the phases, with

*Corresponding author. *Email addresses:* rguo@zzu.edu.cn (R. Guo), yxu@ustc.edu.cn (Y. Xu)

a smooth change between both values in the zone around the interfaces, which is then diffused with a finite width.

In the phase field model, the dynamics of the underlying physical system is generally described by a gradient flow resulting from the Euler-Lagrangian variation of a pre-defined energy form with embedded phase-field functions. However, the gradient flow, in the form of high order stiff partial differential equations (PDEs), poses a great deal of difficulty for numerical simulations [24, 39]. Namely, high resolution simulation is preferred in order to capture the generally sharp interfacial structures and to provide numerical solution with fidelity. In addition, the model itself experiences long time evolution therefore computational efficiency is essential to map out the whole dynamics from initial state to steady state.

Various numerical simulations have been developed for phase field problems recently, especially for temporal discretization, which mostly are the convex splitting schemes [4, 10, 12–14, 18, 19, 21, 23, 27, 28], the stabilized linear schemes [11, 17, 20] and others [1, 29]. In the convex splitting scheme, one first splits the energy into convex and nonconvex parts. Then one discretizes the terms of the variational derivative implicitly for the convex part, and explicitly for the nonconvex part of the energy respectively. The resulting convex splitting schemes are unconditionally energy stable. However, they are nonlinear in most cases, which results in nonlinear systems, hence iterative methods are necessary. Moreover, as for the unique solvability of the nonlinear scheme, the proof is not easy. In some cases, nonlinear schemes also require very small time step to guarantee the unique solvability. While for the stabilized linear scheme, the term from the nonlinear potential is simply treated explicitly and some linear stabilizing terms are added to improve the stability. The resulting linear schemes are simple and easy to implement. However, the energy stability depends on the boundedness of the numerical solution, which is not satisfied for most phase field models. In such case, the stabilized linear scheme fails to preserve the energy stability.

In order to overcome the difficulties mentioned above, one hopes to construct a linear scheme which preserves the energy stability. Yang *et al.* developed a novel scheme based on the invariant energy quadratization (IEQ) approach and have been successfully used to solve the molecular beam epitaxial (MBE) growth model [2, 34], the phase field crystal model [32] and various gradient flows [31, 33, 35–38]. The numerical scheme using the IEQ approach takes the following advantages: 1) It is unconditionally energy stable. 2) It is easy to construct the second order scheme, thus more accurate. 3) It is linear and thus easy to implement and efficient. Inspired by the idea, the IEQ approach can be applied to solve other phase field problems automatically, for example, the Allen-Cahn (AC) equation, the Cahn-Hilliard (CH) equation and the Cahn-Hilliard-Hele-Shaw (CHHS) system. The linear scheme is unconditionally energy stable and easy to implement. However, it is only first order or second order accurate in time, and not straightforward to extend to higher order ones. In this paper, we will apply the semi-implicit spectral deferred correction (SDC) method [15] to improve the temporal accuracy, which borrows the linear unconditionally stable method as the basis scheme. We only pay attention to some clas-

sical and widely used phase field models, namely the AC equation, the CH equation, the MBE growth model and the CHHS system in this paper, it is clear that the technique can be applied to more general gradient flows.

Regarding spatial discretization, the discontinuous Galerkin (DG) method will be developed in this paper. The DG method we discuss here is a finite element method using a completely discontinuous piecewise polynomial space for the numerical solution and the test functions. It was first introduced in 1973 by Reed and Hill [22] for solving the linear time-independent neutron transport equation. Later, the DG method was developed for solving the nonlinear hyperbolic conservation laws by Cockburn *et al.* in a series of papers [5–8].

For PDEs containing higher order spatial derivatives, it is not straightforward to apply the DG method directly, so the local discontinuous Galerkin (LDG) method was introduced. The first LDG method was designed to solve a convection diffusion equation (with second derivatives) by Cockburn and Shu [9]. The idea of LDG methods is to suitably rewrite a higher order PDE into a first order system, then apply the DG method to the system. A key ingredient for the success of such methods is the correct design of interface numerical fluxes, which should be designed to guarantee stability. The DG and LDG methods have several attractive properties, for example: 1) The order of accuracy can be locally determined in each cell, thus allowing for efficient p adaptivity. 2) These methods can be used on arbitrary triangulations, even those with hanging nodes, thus allowing for efficient h adaptivity. 3) These methods have excellent parallel efficiency. With the LDG method for spatial discretization and the semi-implicit SDC method for temporal discretization, it is obvious that we can achieve high order accuracy in both time and space.

Implicit temporal discretization methods lead to linear algebraic equations to solve at each time step, traditional iterative solution methods, such as Gauss-Seidel method, suffers from slow convergence rates, especially for larger system. To further improve the efficiency of the proposed approaches, the multigrid solver is employed to solve the linear algebraic equations at each time step, which converges with optimal or nearly optimal rates.

The organization of the paper is as follows. In Section 2, we develop the unconditionally energy stable linear schemes based on the IEQ approach for a series of phase field problems, including the AC equation, the CH equation, the MBE growth model and the CHHS system. Moreover, we introduce a high order semi-implicit SDC method combining with these linear schemes to achieve high order accuracy in both time and space. Numerical experiments are presented in Section 3, testing the performance of these proposed approaches for solving phase field problems. We give concluding remarks in Section 4. In Appendices A and B, we take the AC equation as an example to prove the unconditional energy stability of the proposed linear scheme when coupled with the LDG spatial discretization method.

2 Semi-implicit SDC schemes based on the IEQ approach

In [34], Yang *et al.* presented a first order stable scheme based on the IEQ method for the MBE growth models. The novelty is that all nonlinear terms are treated semi-explicitly, and the resulted semi-discrete equations form a linear system at each time step. In this section, we will first focus on constructing the corresponding linear unconditionally stable schemes based on the IEQ approach for the AC equation, the CH equation and the CHHS system.

The proposed schemes are all linear and unconditionally energy stable, namely, they are stable regardless of time step size. However, these schemes are only first order accurate in time. To improve the temporal accuracy, we will then employ the semi-implicit spectral deferred correction (SDC) method [15].

The novelty is how to combine SDC method with the proposed linear schemes developed by IEQ approach to maintain the expected high order accuracy of SDC method.

2.1 SDC scheme for the Allen-Cahn equation

2.1.1 The first order linear scheme

We consider the Allen-Cahn equation with degenerate mobility

$$\phi_t = b(\phi)(\varepsilon^2\Delta\phi - F'(\phi)), \tag{2.1}$$

where $b(\phi)\geq 0$ is the degenerate mobility and $F(\phi)=\frac{1}{4}(\phi^2-1)^2$. The Allen-Cahn equation (2.1) is a gradient flow in L^2 with the free energy

$$E(\phi)=\int_\Omega \left(\frac{1}{2}\varepsilon^2|\nabla\phi|^2+F(\phi)\right)d\boldsymbol{x}. \tag{2.2}$$

Inspired by the IEQ approach [32, 34] to discrete the nonlinear term ϕ^3, we introduce the auxiliary function as follows

$$U=\phi^2-1. \tag{2.3}$$

Then, we can recast the free energy (2.2) as a quadratic function of ϕ and U

$$E(\phi,U)=\int_\Omega \left(\frac{1}{2}\varepsilon^2|\nabla\phi|^2+\frac{1}{4}U^2\right)d\boldsymbol{x}, \tag{2.4}$$

and the equivalent equation is given as

$$\phi_t = b(\phi)(\varepsilon^2\Delta\phi - \phi U), \tag{2.5}$$

$$U_t = 2\phi\phi_t. \tag{2.6}$$

The initial conditions are

$$\phi(t=0)=\phi_0, \quad U(t=0)=\phi_0^2-1.$$

Further, the equivalent equation preserves an energy law, namely,

$$\frac{d}{dt}E(\phi,U)=-\int_\Omega b(\phi)(-\varepsilon^2\Delta\phi+\phi U)^2 d\boldsymbol{x}\leq 0. \tag{2.7}$$

Obviously, we hope to construct a linear scheme that preserve the energy law (2.7) in the discrete level. A first order linear scheme for solving the system (2.5)-(2.6) can be given as follows

$$\frac{\phi^{n+1}-\phi^n}{\Delta t}=b(\phi^n)(\varepsilon^2\Delta\phi^{n+1}-\phi^n U^{n+1}), \tag{2.8}$$

$$\frac{U^{n+1}-U^n}{\Delta t}=2\phi^n\frac{\phi^{n+1}-\phi^n}{\Delta t}. \tag{2.9}$$

Since (2.9) is a simple algebraic equation, we can rewrite it as

$$U^{n+1}=U^n+2\phi^n(\phi^{n+1}-\phi^n). \tag{2.10}$$

Then the linear scheme (2.8)-(2.9) can be written as

$$\frac{\phi^{n+1}-\phi^n}{\Delta t}=b(\phi^n)(\varepsilon^2\Delta\phi^{n+1}-\phi^n(U^n+2\phi^n(\phi^{n+1}-\phi^n))). \tag{2.11}$$

Thus, we can solve ϕ^{n+1} directly from (2.11), which means that the auxiliary U does not indeed increase the computational costs. However, it will lead to solving linear equations with complicated variable coefficients, which is a drawback of the IEQ approach.

Remark 2.1. For spatial discretization, we use the LDG method. In Appendices A and B, we will take the AC equation as an example to illustrate the LDG method to solve the linear scheme (2.8)-(2.9) and prove the corresponding energy stability.

2.1.2 The high order SDC scheme

The SDC method is a special case of the DC (deferred correction) method [25], and it is driven iteratively by the chosen first order linear scheme (2.8)-(2.9). An advantage of SDC method is that it is a one step method and can be constructed easily and systematically for any order of accuracy.

Suppose now the time interval $[0,T]$ is divided into M non-overlapping intervals by the partition $0=t_0<t_1<\cdots<t_n<\cdots<t_M=T$. We shall describe below the semi-implicit SDC method which will be used to advance from t_n to t_{n+1}. Let $\Delta t_n=t_{n+1}-t_n$ and ϕ_n denotes the numerical approximation of $\phi(t_n)$, with $\phi_0=\phi(0)$.

Divide the time interval $[t_n,t_{n+1}]$ into P subintervals by choosing the points $t_{n,m}$ for $m=0,1,\cdots,P$ such that $t_n=t_{n,0}<t_{n,1}<\cdots<t_{n,m}<\cdots<t_{n,P}=t_{n+1}$. Let $\Delta t_{n,m}=t_{n,m+1}-t_{n,m}$ and $\phi^k_{n,m}$ denotes the k^{th} order approximation to $\phi(t_{n,m})$. The points $\{t_{n,m}\}_{m=0}^P$ can be chosen to be the Chebyshev Gauss-Lobatto nodes on $[t_n,t_{n+1}]$ to avoid the instability of approximation at equispaced nodes for high order accuracy. We can also choose the Gauss nodes,

or Legendre Gauss-Radau nodes or Legendre Gauss-Lobatto nodes. Starting from ϕ_n, U_n, we give the algorithm to calculate ϕ_{n+1}, U_{n+1} in the following.

Compute the initial approximation based on first order scheme:

$$\phi^1_{n,0}=\phi_n,\quad U^1_{n,0}=U_n.$$

Use the first order linear scheme (2.8)-(2.9) to compute approximate solution ϕ^1,U^1 at the nodes $\{t_{n,m}\}_{m=1}^P$, *i.e.*

For $m=0,\cdots,P-1$

$$\phi^1_{n,m+1}=\phi^1_{n,m}+\Delta t_{n,m}b(\phi^1_{n,m})(\varepsilon^2\Delta\phi^1_{n,m+1}-\phi^1_{n,m}U^1_{n,m+1}), \tag{2.12}$$

$$\frac{U^1_{n,m+1}-U^1_{n,m}}{\Delta t}=2\phi^1_{n,m}\frac{\phi^1_{n,m+1}-\phi^1_{n,m}}{\Delta t}. \tag{2.13}$$

Compute successive corrections:

For $k=1,\cdots,K$

$$\phi^{k+1}_{n,0}=\phi_n,\quad U^{k+1}_{n,0}=U_n.$$

For $m=0,\cdots,P-1$

$$\begin{aligned}\phi^{k+1}_{n,m+1}=&\phi^{k+1}_{n,m}+\Delta t_{n,m}b(\phi^k_{n,m+1})[(\varepsilon^2\Delta\phi^{k+1}_{n,m+1}-\phi^{k+1}_{n,m+1}U^k_{n,m+1})\\&-(\varepsilon^2\Delta\phi^k_{n,m+1}-\phi^k_{n,m+1}U^k_{n,m+1})]+I^{m+1}_m(F(t,\phi^k,\phi^k,U^k)),\end{aligned} \tag{2.14}$$

$$U^{k+1}_{n,m+1}=(\phi^{k+1}_{n,m+1})^2-1, \tag{2.15}$$

where

$$F(t,\phi^k,\phi^k,U^k)=b(\phi^k)(\varepsilon^2\Delta\phi^k-\phi^kU^k),$$

and $I^{m+1}_m(F(t,\phi^k,\phi^k,U^k))$ is the integral of the P-th degree interpolating polynomial on the $P+1$ points $(t_{n,m},F(t_{n,m},\phi^k_{n,m},\phi^k_{n,m},U^k_{n,m}))_{m=0}^P$ over the subinterval $[t_{n,m},t_{n,m+1}]$. The details of how to compute $I^{m+1}_m(F(t,\phi^k,\phi^k,U^k))$ was specified in [15].

Finally we have $\phi_{n+1}=\phi^{K+1}_{n,P}$ and $U_{n+1}=U^{K+1}_{n,P}$.

Remark 2.2. In the correction procedure of the above algorithm, the approximation of $U^{k+1}_{n,m+1}$ with the form (2.15) is employed here to maintain the high order temporal accuracy, which is different from the first order scheme (2.13).

2.2 SDC scheme for the Cahn-Hilliard equation

The Cahn-Hilliard equation

$$\phi_t=\nabla\cdot(b(\phi)\nabla(-\varepsilon^2\Delta\phi+F'(\phi))) \tag{2.16}$$

is a gradient flow in H^{-1} with the free energy

$$E(\phi)=\int_\Omega\left(\frac{1}{2}\varepsilon^2|\nabla\phi|^2+F(\phi)\right)dx, \tag{2.17}$$

where $F(\phi)=\frac{1}{4}(\phi^2-1)^2$.

To develop a linear scheme based on the IEQ approach, we introduce the auxiliary functions

$$U=\phi^2-1, \quad \mu=-\varepsilon^2\Delta\phi,$$

and then construct the following first order linear scheme

$$\frac{\phi^{n+1}-\phi^n}{\Delta t}=\nabla\cdot(b(\phi^n)\nabla(\mu^{n+1}+\phi^n U^{n+1})), \tag{2.18}$$

$$\mu^{n+1}=-\varepsilon^2\Delta\phi^{n+1}, \tag{2.19}$$

$$\frac{U^{n+1}-U^n}{\Delta t}=2\phi^n\frac{\phi^{n+1}-\phi^n}{\Delta t}. \tag{2.20}$$

The first order linear scheme (2.18)-(2.20) also preserves the discrete energy stability.

Remark 2.3. Similarly, we can develop the semi-implicit SDC schemes based on the corresponding first order linear scheme (2.18)-(2.20) for the Cahn-Hilliard equation, where we introduce the same auxiliary function $U=\phi^2-1$.

2.3 SDC scheme for the Cahn-Hilliard-Hele-Shaw system

We consider the CHHS system

$$\begin{cases}\phi_t=\Delta\mu+\nabla\cdot(\phi(\nabla p+\gamma\phi\nabla\mu)),\\ \mu=\phi^3-\phi-\varepsilon^2\Delta\phi,\\ -\Delta p=\gamma\nabla\cdot(\phi\nabla\mu),\end{cases} \tag{2.21}$$

which is mass conservative and energy dissipative, *i.e.*

$$\frac{d}{dt}E=-\int_\Omega\left(|\nabla\mu|^2+\frac{1}{\gamma}|\boldsymbol{u}|^2\right)d\boldsymbol{x}\le 0, \tag{2.22}$$

where

$$E(\phi)=\int_\Omega\left(\frac{1}{4}\phi^4-\frac{1}{2}\phi^2+\frac{\varepsilon^2}{2}|\nabla\phi|^2\right)d\boldsymbol{x}, \quad \text{and} \quad \boldsymbol{u}=-\nabla p-\gamma\phi\nabla\mu.$$

Introduce the auxiliary function

$$U=\phi^2-1,$$

we can achieve the following first order linear scheme

$$\begin{cases}\dfrac{\phi^{n+1}-\phi^n}{\Delta t}=\Delta\mu^{n+1}+\nabla\cdot(\phi^n(\nabla p^{n+1}+\gamma\phi^n\nabla\mu^{n+1})),\\ \mu^{n+1}=\phi^n U^{n+1}-\varepsilon^2\Delta\phi^{n+1},\\ -\Delta p^{n+1}=\gamma\nabla\cdot(\phi^n\nabla\mu^{n+1}),\\ \dfrac{U^{n+1}-U^n}{\Delta t}=2\phi^n\dfrac{\phi^{n+1}-\phi^n}{\Delta t}.\end{cases} \tag{2.23}$$

The scheme (2.23) is unconditionally energy stable. In addition, to the best of the authors' knowledge, this is the first linear scheme with energy stability result for the CHHS system.

Remark 2.4. The semi-implicit SDC scheme based on the corresponding first order linear scheme (2.23) for the Cahn-Hilliard-Hele-Shaw system can be developed similarly as before, we will omit the details here.

2.4 SDC schemes for the molecular beam epitaxial growth models

The molecular beam epitaxial (MBE) growth model is the gradient flow with the energy

$$E(\phi)=\int_\Omega\left(\frac{1}{2}\varepsilon^2|\Delta\phi|^2+F(\nabla\phi)\right)d\boldsymbol{x}, \tag{2.24}$$

where for the MBE model without slope selection, $F(\nabla\phi)$ is given as

$$F(\nabla\phi)=-\frac{1}{2}\ln(|\nabla\phi|^2+1),$$

and for the MBE model with slope selection, $F(\nabla\phi)$ reads

$$F(\nabla\phi)=\frac{1}{4}(|\nabla\phi|^2-1)^2.$$

Therefore, the gradient flow for the MBE model without slope selection follows

$$\phi_t=-b(\phi)\left(\varepsilon^2\Delta^2\phi+\nabla\cdot\left(\frac{1}{1+|\nabla\phi|^2}\nabla\phi\right)\right), \tag{2.25}$$

and the gradient flow for the MBE model with slope selection is given by

$$\phi_t=-b(\phi)\left(\varepsilon^2\Delta^2\phi-\nabla\cdot((|\nabla\phi|^2-1)\nabla\phi)\right). \tag{2.26}$$

Followed the IEQ approach suggested in [34], we present the corresponding first order linear schemes as follows.

2.4.1 The MBE model without slope selection

Introduce the auxiliary functions

$$U=\sqrt{\ln(1+|\nabla\phi|^2)+1},\quad \mu=-\varepsilon^2\Delta\phi,$$

and the equivalent PDE system reads as follows

$$\phi_t=b(\phi)(\Delta\mu-\nabla\cdot(U\boldsymbol{H})), \tag{2.27}$$
$$\mu=-\varepsilon^2\Delta\phi, \tag{2.28}$$
$$U_t=\boldsymbol{H}\cdot\nabla\phi_t, \tag{2.29}$$

where

$$\boldsymbol{H}=\frac{\nabla\phi}{(1+|\nabla\phi|^2)\sqrt{\ln(1+|\nabla\phi|^2)+1}}.$$

The first order linear scheme to solve the system (2.27)-(2.29) is

$$\frac{\phi^{n+1}-\phi^n}{\Delta t}=b(\phi^n)(\Delta\mu^{n+1}-\nabla\cdot(U^n\boldsymbol{H}^n)), \tag{2.30}$$

$$\mu^{n+1}=-\varepsilon^2\Delta\phi^{n+1}, \tag{2.31}$$

$$\frac{U^{n+1}-U^n}{\Delta t}=\boldsymbol{H}^n\cdot\nabla\frac{\phi^{n+1}-\phi^n}{\Delta t}, \tag{2.32}$$

where

$$\boldsymbol{H}^n=\frac{\nabla\phi^n}{(1+|\nabla\phi^n|^2)\sqrt{\ln(1+|\nabla\phi^n|^2)+1}}.$$

2.4.2 The MBE model with slope selection

We introduce the auxiliary functions

$$V=|\nabla\phi|^2-1,\quad \mu=-\varepsilon^2\Delta\phi,$$

and the equivalent PDE system reads as follows

$$\phi_t=b(\phi)(\Delta\mu+\nabla\cdot(V\nabla\phi)), \tag{2.33}$$

$$\mu=-\varepsilon^2\Delta\phi, \tag{2.34}$$

$$V_t=2\nabla\phi\cdot\nabla\phi_t. \tag{2.35}$$

The first order linear scheme to solve the system (2.33)-(2.35) is

$$\frac{\phi^{n+1}-\phi^n}{\Delta t}=b(\phi^n)(\Delta\mu^{n+1}+\nabla\cdot(V^{n+1}\nabla\phi^n)), \tag{2.36}$$

$$\mu^{n+1}=-\varepsilon^2\Delta\phi^{n+1}, \tag{2.37}$$

$$\frac{V^{n+1}-V^n}{\Delta t}=2\nabla\phi^n\cdot\nabla\frac{\phi^{n+1}-\phi^n}{\Delta t}. \tag{2.38}$$

Remark 2.5. The linear schemes (2.30)-(2.32) and (2.36)-(2.38) both preserve the corresponding discrete energy stability.

2.4.3 The high order SDC schemes

For the MBE model with slope selection, the initial approximation and the successive corrections are almost the same with above, except that we replace equation (2.15) by

$$V_{n,m+1}^{k+1}=|\nabla\phi_{n,m+1}^{k+1}|^2-1.$$

While for the MBE model without slope selection, the semi-implicit SDC scheme is as follows.

Compute the initial approximation based on first order scheme:

$$\phi^1_{n,0}=\phi_n,\quad \mu^1_{n,0}=\mu_n,\quad U^1_{n,0}=U_n,\quad \boldsymbol{H}^1_{n,0}=\boldsymbol{H}_n.$$

For $m=0,\cdots,P-1$

$$\begin{aligned}
&\phi^1_{n,m+1}=\phi^1_{n,m}+\Delta t_{n,m}b(\phi^1_{n,m})(\Delta\mu^1_{n,m+1}-\nabla\cdot(U^1_{n,m}\boldsymbol{H}^1_{n,m})),\\
&\mu^1_{n,m+1}=-\varepsilon^2\Delta\phi^1_{n,m+1},\\
&\frac{U^1_{n,m+1}-U^1_{n,m}}{\Delta t}=\boldsymbol{H}^1_{n,m}\cdot\nabla\frac{\phi^1_{n,m+1}-\phi^1_{n,m}}{\Delta t}.
\end{aligned}$$

Compute successive corrections:

For $k=1,\cdots,K$

$$\phi^{k+1}_{n,0}=\phi_n,\quad \mu^{k+1}_{n,0}=\mu_n,\quad U^{k+1}_{n,0}=U_n,\quad \boldsymbol{H}^{k+1}_{n,0}=\boldsymbol{H}_n.$$

For $m=0,\cdots,P-1$

$$\begin{aligned}
&\phi^{k+1}_{n,m+1}=\phi^{k+1}_{n,m}+\Delta t_{n,m}b(\phi^k_{n,m+1})(\Delta\mu^{k+1}_{n,m+1}-\Delta\mu^k_{n,m+1})+I^{m+1}_m(F(t,\phi^k,\mu^k,U^k,\boldsymbol{H}^k)),\\
&\mu^{k+1}_{n,m+1}=-\varepsilon^2\Delta\phi^{k+1}_{n,m+1},\\
&U^{k+1}_{n,m+1}=\sqrt{\ln(1+|\nabla\phi^{k+1}_{n,m+1}|^2)+1},\\
&\boldsymbol{H}^{k+1}_{n,m+1}=\frac{\nabla\phi^{k+1}_{n,m+1}}{(1+|\nabla\phi^{k+1}_{n,m+1}|^2)U^{k+1}_{n,m+1}},
\end{aligned}$$

where

$$F(t,\phi^k,\mu^k,U^k,\boldsymbol{H}^k)=b(\phi^k)(\Delta\mu^k-\nabla\cdot(U^k\boldsymbol{H}^k)).$$

Finally we have $\phi_{n+1}=\phi^{K+1}_{n,P}$, $\mu_{n+1}=\mu^{K+1}_{n,P}$, $U_{n+1}=U^{K+1}_{n,P}$ and $\boldsymbol{H}_{n+1}=\boldsymbol{H}^{K+1}_{n,P}$.

Remark 2.6. (Local truncation error). The local truncation error obtained with the semi-implicit SDC^P_K scheme based on the IEQ approach is [15]

$$\mathcal{O}(h^{\min[K+1,P+1]}),\tag{2.39}$$

where $h=\max_{n,m}\Delta t_{n,m}$.

Remark 2.7. The proposed first order linear schemes (2.8)-(2.9), (2.18)-(2.20), (2.23), (2.30)-(2.32) and (2.36)-(2.38) are all based on the IEQ approach. The novelty here is how to combine the semi-implicit SDC method with these linear schemes to maintain the expected high order accuracy of the SDC method.

Remark 2.8. From the numerical experiments in the next section, it can be found that the SDC method based on the linear scheme can maintain the energy stability numerically. For the semi-implicit SDC scheme, the iteration and the left-most endpoint involved in the integral for the implicit part increase the difficulty of the energy stability analysis. The energy equations are more difficult to construct, compared with the first order scheme or the Runge-Kutta type semi-implicit schemes. It is not easy to prove the energy stability of the semi-implicit SDC scheme for phase field models. We will leave it as our future work.

Remark 2.9. The semi-implicit SDC methods lead to linear algebraic equations to solve at each iteration, and the overall performance of the SDC method highly depends on the efficiency of the linear solver. To enhance the efficiency of the high order semi-implicit time marching method, we will apply the multigrid solver to solve them in this paper. For a detailed description of the multigrid solver [26,30] coupled with LDG spatial discretization, we refer readers to our recent work [12], which presents numerical experiments to show that the multigrid solver have optimal or nearly optimal convergence rates.

3 Numerical results

In this section, we present some numerical experiments for solving the AC equation, the CH equation, the MBE growth models and the CHHS system. The spatial discretization method is LDG scheme and the temporal discretization technique is the energy stable linear schemes combined with the semi-implicit SDC scheme. We perform a series of accuracy tests, which show the expected high order accuracy in both time and space. In addition, we present some long time simulation examples to show the capability of the semi-implicit SDC method based on the IEQ approach and the energy stability results of the proposed methods.

The Allen-Cahn equation

We consider the Allen-Cahn equation with $b(\phi)=1-\phi^2$, $\varepsilon=1.0$ in the square domain $\Omega=[0,2\pi]\times[0,2\pi]$ and with periodic boundary condition. To verify the convergence rate, we choose the suitable forcing function so that the exact solution is given by

$$\phi(x,y,t)=e^{-2t}\sin(x)\sin(y). \tag{3.1}$$

We use the LDG method for spatial discretization on the uniform mesh with the cell size $\Delta x=\Delta y=2\pi/N$.

Temporal accuracy test. To test the temporal accuracy of the SDC method, we choose $\mathcal{P}^4$ approximation and $N=128$ to ensure that the spatial discretization error is small enough, such that the temporal discretization error is dominant. We present the L^2 and

L^∞ errors and the numerical orders of temporal accuracy in Table 1, which shows the expected accuracy of the SDC method.

Table 1: Temporal accuracy test for the Allen-Cahn equation with the exact solution (3.1) at time $T=0.5$. Here we choose $\Delta x=2\pi/128$ and piecewise $\mathcal{P}^4$ approximations. The refinement path is $\Delta t=\Delta t_0/2^m$, $m=0,1,2,3$ and $\Delta t_0=0.0375$.

	m	L^2 error	order	L^∞ error	order
SDC_2^0	0	2.33E-02	–	7.46E-03	–
	1	1.21E-02	0.95	3.89E-03	0.94
	2	6.19E-03	0.97	1.98E-03	0.97
	3	3.12E-03	0.99	1.00E-03	0.99
SDC_2^1	0	4.12E-04	–	1.27E-04	–
	1	1.11E-04	1.89	3.43E-05	1.89
	2	2.90E-05	1.94	8.93E-06	1.94
	3	7.39E-06	1.97	2.27E-06	1.98
SDC_2^2	0	4.26E-06	–	1.25E-06	–
	1	6.90E-07	2.63	2.02E-07	2.63
	2	9.73E-08	2.83	2.97E-08	2.77
	3	1.30E-08	2.90	4.23E-09	2.81

Spatial and temporal accuracy test. To show that the proposed space and time discretization methods are high order accurate, we use the piecewise $\mathcal{P}^r$ approximations for spatial discretization and the SDC_3^3 method for temporal discretization. Table 2 presents the L^2 and L^∞ errors and the numerical orders of accuracy at time $T=0.5$, which shows $(r+1)$-th order of accuracy for $\mathcal{P}^r$ approximation.

Table 2: Spatial and temporal accuracy test for the Allen-Cahn equation with the exact solution (3.1) at time $T=0.5$. Here we choose the SDC_3^3 method with $\Delta t=0.1\Delta x$ and $\Delta x=2\pi/N$.

	N	L^2 error	order	L^∞ error	order
$\mathcal{P}^0$	16	1.84E-01	–	6.47E-02	–
	32	9.25E-02	0.99	3.27E-02	0.98
	64	4.63E-02	1.00	1.63E-02	1.00
$\mathcal{P}^1$	16	2.12E-02	–	1.52E-02	–
	32	5.33E-03	2.00	3.86E-03	1.98
	64	1.33E-03	2.00	9.69E-04	2.00
$\mathcal{P}^2$	16	1.35E-03	–	1.25E-03	–
	32	1.69E-04	3.00	1.55E-04	3.01
	64	2.11E-05	3.00	1.92E-05	3.01
$\mathcal{P}^3$	16	6.80E-05	–	8.63E-05	–
	32	4.25E-06	4.00	5.51E-06	3.97
	64	2.66E-07	4.00	3.47E-07	3.99

Convergence and complexity of the multigrid solver. To demonstrate the near optimal complexity (with respect to the spatial step size Δx) of the multigrid solver, we provide evidence that the multigrid convergence rate is nearly independent of Δx. We fix the time step as $\Delta t = 0.01\Delta x$ and the spatial step size varies from $\Delta x = 2\pi/32$ to $\Delta x = 2\pi/128$. The convergence rates of the multigrid solver at the 10th time step is presented in Fig. 1, we can see the nearly optimal convergence of the solver.

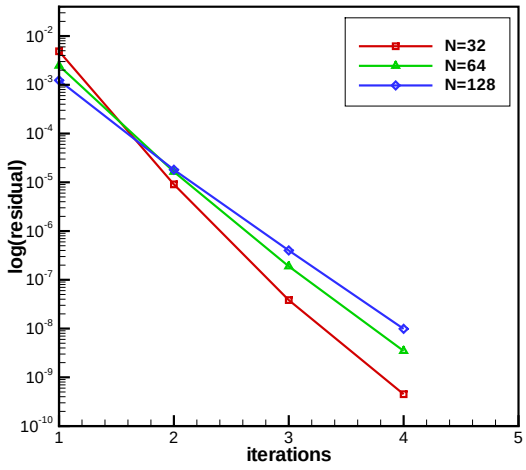

Figure 1: Convergence rates of multigrid solver with $\mathcal{P}^2$ approximation for the Allen-Cahn equation.

Spinodal decomposition. Here we present an example of spinodal decomposition. We consider the piecewise $\mathcal{P}^2$ approximations for spatial discretization and the SDC_2^2 method for temporal discretization with $\Delta t = 0.1\Delta x$. The initial data is a random number varying from -0.01 to 0.01. The domain is $[0,2\pi]\times[0,2\pi]$ and ε is fixed as 0.1. Fig. 2 shows the corresponding numerical simulations. In spinodal decomposition, particles can coarsen, *i.e.* large particles may grow at the expense of smaller particles. The energy evolution with $\Delta t = 0.1\Delta x$ is presented in Fig. 3, which shows the energy is decreasing, namely, the SDC method is energy stable numerically.

The Cahn-Hilliard equation

Spatial and temporal accuracy test. We consider the Cahn-Hilliard equation with $b(\phi) = 1-\phi^2$, $\varepsilon = 1.0$ in the square domain $\Omega = [0,2\pi]\times[0,2\pi]$ and with periodic boundary condition. To verify the convergence rate, we choose the suitable forcing function so that the exact solution is given by

$$\phi(x,y,t) = e^{-2t}\sin(x)\sin(y). \tag{3.2}$$

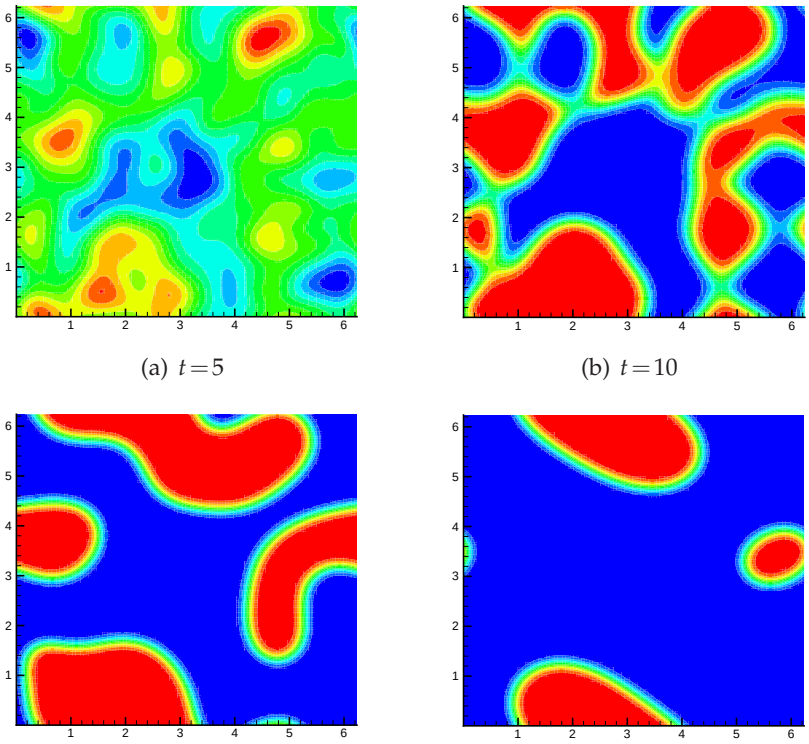

(a) $t=5$ (b) $t=10$

(c) $t=30$ (d) $t=100$

Figure 2: Numerical results of the Allen-Cahn equation using the piecewise $\mathcal{P}^2$ approximation and the SDC_2^2 method with $\Delta t=0.1\Delta x$.

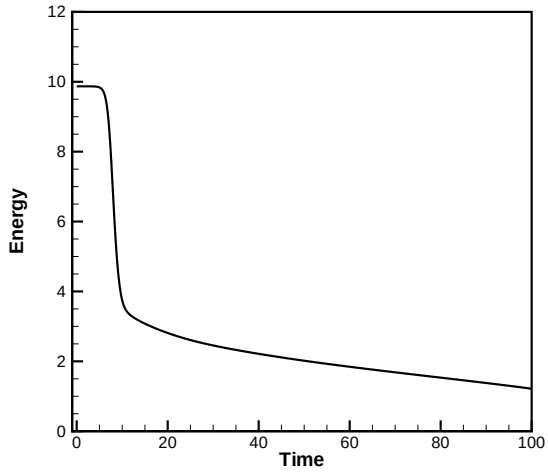

Figure 3: Energy evolution of the SDC_2^2 method with $\Delta t=0.1\Delta x$ for the Allen-Cahn equation.

We choose the piecewise $\mathcal{P}^r$ approximations for spatial discretization and the SDC_3^3 method for temporal discretization. The L^2 and L^∞ errors and the numerical orders of accuracy at time $T=0.5$ is presented in Table 3, which indicates the optimal $(r+1)$-th order of accuracy for $\mathcal{P}^r$ approximation.

Table 3: Spatial and temporal accuracy test for the Cahn-Hilliard equation with the exact solution (3.2) at time $T=0.5$. Here we choose the SDC_3^3 method with $\Delta t=0.1\Delta x$ and $\Delta x=2\pi/N$.

	N	L^2 error	order	L^∞ error	order
$\mathcal{P}^0$	16	1.93E-01	–	7.78E-02	–
	32	9.50E-02	1.02	3.79E-02	1.04
	64	4.72E-02	1.01	1.86E-02	1.02
$\mathcal{P}^1$	16	2.12E-02	–	1.52E-02	–
	32	5.33E-03	2.00	3.85E-03	1.98
	64	1.33E-03	2.00	9.66E-04	1.99
$\mathcal{P}^2$	16	1.40E-03	–	1.24E-03	–
	32	1.71E-04	3.03	1.55E-04	3.01
	64	2.12E-05	3.01	1.94E-05	3.00
$\mathcal{P}^3$	16	6.80E-05	–	8.74E-05	–
	32	4.27E-06	3.99	5.68E-06	3.94
	64	2.76E-07	3.95	3.66E-07	3.96

The convergence rates of the multigrid solver implemented with $\Delta t=0.001$ at the 10th time step is presented in Fig. 4, which shows the optimal convergence rate.

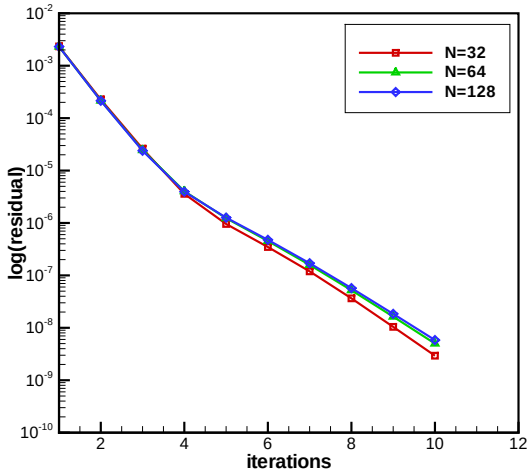

Figure 4: Convergence rates of multigrid solver with $\mathcal{P}^2$ approximation for the Cahn-Hilliard equation.

Long time simulation. We consider the Cahn-Hilliard equation with $\varepsilon = 0.1$ in the square domain $[0,2\pi]\times[0,2\pi]$. The initial data is

$$\phi(x,y,0) = 0.1(\sin 3x \sin 2y + \sin 5x \sin 5y).$$

The computational parameters are the spatial discretization cell size $\Delta x = 2\pi/N$ with $N = 128$ and the piecewise $\mathcal{P}^2$ approximation. The numerical results are shown in Fig. 5. The energy evolution with $\Delta t = 0.1\Delta x$ is presented in Fig. 6, which shows the energy is decreasing, namely, the SDC method is energy stable numerically.

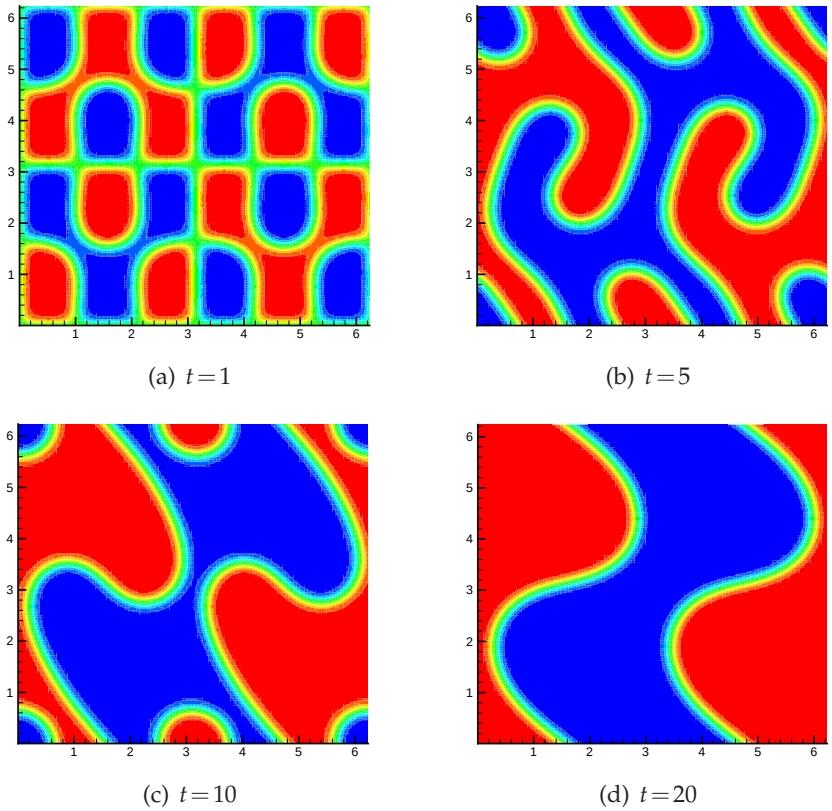

(a) $t = 1$ (b) $t = 5$

(c) $t = 10$ (d) $t = 20$

Figure 5: Numerical results of the Cahn-Hilliard equation using the piecewise $\mathcal{P}^2$ approximation and the SDC_2^2 method with $\Delta t = 0.1\Delta x$.

The molecular beam epitaxial growth models

Spatial and temporal accuracy test. We consider the molecular beam epitaxial growth models with $b(\phi) = 1-\phi^2$, $\varepsilon = 1.0$ in the square domain $\Omega = [0,2\pi]\times[0,2\pi]$ and with periodic boundary condition. To verify the convergence rate, we choose the suitable forcing

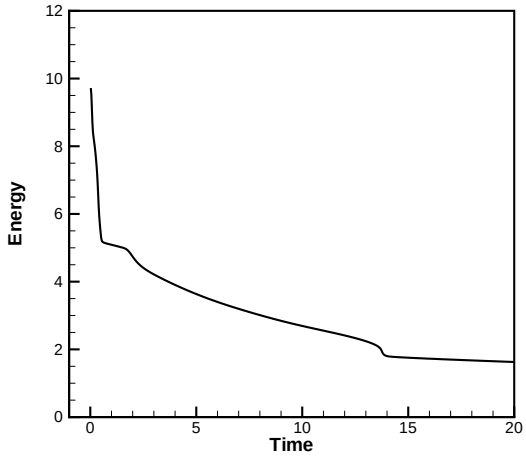

Figure 6: Energy evolution of the SDC_2^2 method with $\Delta t=0.1\Delta x$ for the Cahn-Hilliard equation.

function so that the exact solution is given by

$$\phi(x,y,t)=e^{-2t}\sin(x)\sin(y). \tag{3.3}$$

We choose the piecewise $\mathcal{P}^r$ approximations for spatial discretization and the SDC_3^3 method for temporal discretization. The L^2 and L^∞ errors and the numerical orders of accuracy at time $T=0.5$ for the MBE model without slope selection is presented in Table 4, and the corresponding results for the MBE model with slope selection is presented in Table 5. In both cases, $\mathcal{P}^r$ approximations provide the optimal $(r+1)$-th order of accuracy.

Table 4: Spatial and temporal accuracy test for the MBE model without slope selection at time $T=0.5$. Here we choose the SDC_3^3 method with $\Delta t=0.1\Delta x$ and $\Delta x=2\pi/N$.

	N	L^2 error	order	L^∞ error	order
$\mathcal{P}^0$	16	1.87E-01	–	6.80E-02	–
	32	9.28E-02	1.01	3.34E-02	1.02
	64	4.63E-02	1.00	1.65E-02	1.02
$\mathcal{P}^1$	16	2.12E-02	–	1.51E-02	–
	32	5.33E-03	1.99	3.84E-03	1.98
	64	1.33E-03	2.00	9.65E-04	1.99
$\mathcal{P}^2$	16	1.39E-03	–	1.24E-03	–
	32	1.70E-04	3.03	1.54E-04	3.01
	64	2.12E-05	3.00	1.95E-05	2.98
$\mathcal{P}^3$	16	6.80E-05	–	8.68E-05	–
	32	4.26E-06	4.00	5.58E-06	3.96
	64	2.67E-07	4.00	3.55E-07	3.97

Table 5: Spatial and temporal accuracy test for the MBE model with slope selection at time $T=0.5$. Here we choose the SDC_3^3 method with $\Delta t=0.1\Delta x$ and $\Delta x=2\pi/N$.

	N	L^2 error	order	L^∞ error	order
$\mathcal{P}^0$	16	1.87E-01	–	6.86E-02	–
	32	9.29E-02	1.01	3.36E-02	1.03
	64	4.63E-02	1.00	1.66E-02	1.02
$\mathcal{P}^1$	16	2.12E-02	–	1.51E-02	–
	32	5.33E-03	1.99	3.83E-03	1.98
	64	1.33E-03	2.00	9.64E-04	1.99
$\mathcal{P}^2$	16	1.42E-03	–	1.25E-03	–
	32	1.72E-04	3.05	1.56E-04	3.01
	64	2.13E-05	3.01	1.94E-05	3.01
$\mathcal{P}^3$	16	6.86E-05	–	8.85E-05	–
	32	4.37E-06	3.97	5.77E-06	3.94
	64	2.90E-07	3.91	3.67E-07	3.97

The convergence rates of the multigrid solver implemented with $\Delta t=0.001$ at the 10th time step is presented in Fig. 7, we can see the optimal or near optimal complexity (with respect to the spatial step size Δx) of the multigrid solver.

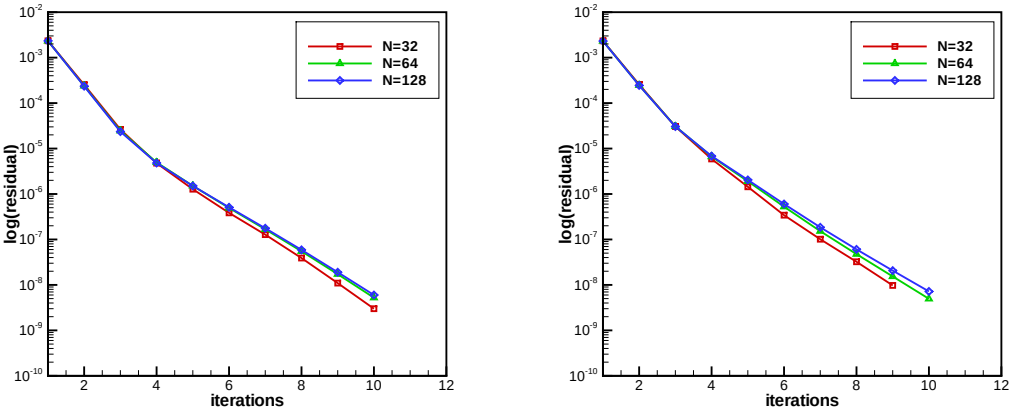

(a) MBE model without slope selection. (b) MBE model with slope selection.

Figure 7: Convergence rates of multigrid solver with $\mathcal{P}^2$ approximation for the MBE models.

Coarsening dynamics. We consider the MBE models with $b(u)=1,\varepsilon=0.1$ in the square domain $[0,12.8]\times[0,12.8]$. The initial data is a random number varying from -0.001 to 0.001. The computational parameters are the spatial discretization cell size $\Delta x=12.8/N$

with $N=128$, the piecewise $\mathcal{P}^2$ approximation and the SDC_2^2 method for temporal discretization. The numerical results are shown in Fig. 8 and Fig. 9 for the MBE models without slope selection and with slope selection, respectively. The energy evolution is presented in Fig. 10, which shows the energy is decreasing, namely, the SDC method is energy stable numerically when solving the MBE models.

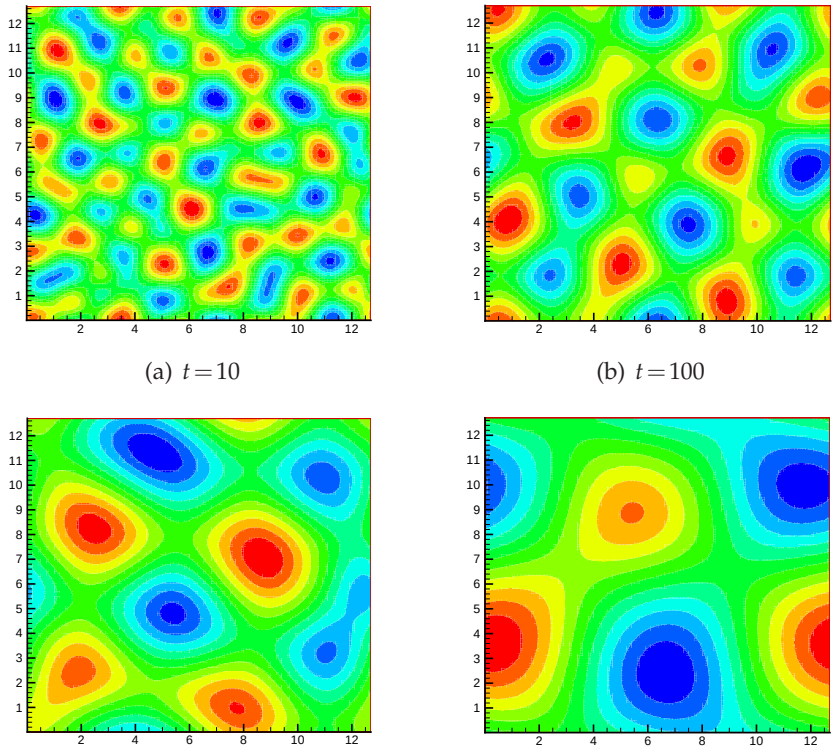

(a) $t=10$ (b) $t=100$

(c) $t=400$ (d) $t=5000$

Figure 8: Numerical results of the MBE model without slope selection using the piecewise $\mathcal{P}^2$ approximation and the SDC_2^2 method.

The Cahn-Hilliard-Hele-Shaw system

Spatial and temporal accuracy test. We consider the Cahn-Hilliard-Hele-Shaw system with $\varepsilon=1.0$, $\gamma=4\varepsilon$ in the square domain $\Omega=[0,2\pi]\times[0,2\pi]$ and with periodic boundary condition. To verify the convergence rate, we choose the suitable forcing function so that the exact solution is given by

$$\phi(x,y,t)=e^{-2t}\sin(x)\sin(y). \tag{3.4}$$

We use the LDG method with piecewise $\mathcal{P}^r$ polynomial basis for spatial discretization

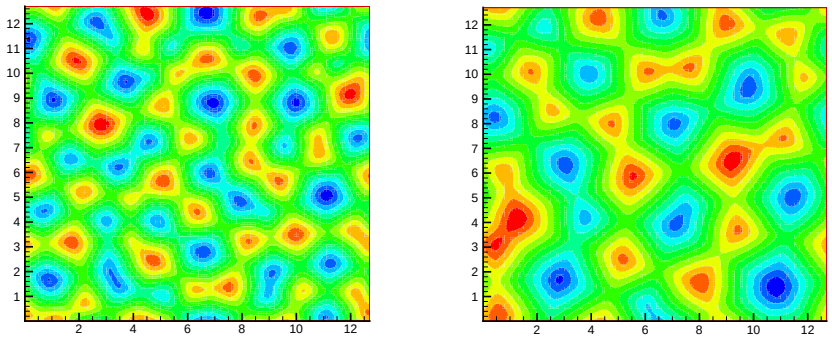

(a) $t=10$ (b) $t=50$

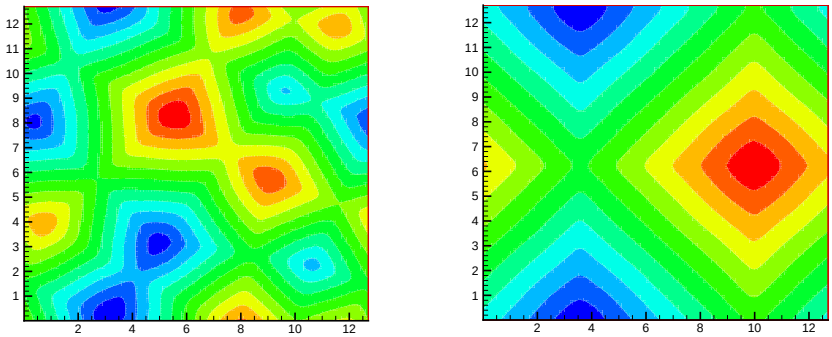

(c) $t=400$ (d) $t=2000$

Figure 9: Numerical results of the MBE model with slope selection using the piecewise $\mathcal{P}^2$ approximation and the SDC_2^2 method.

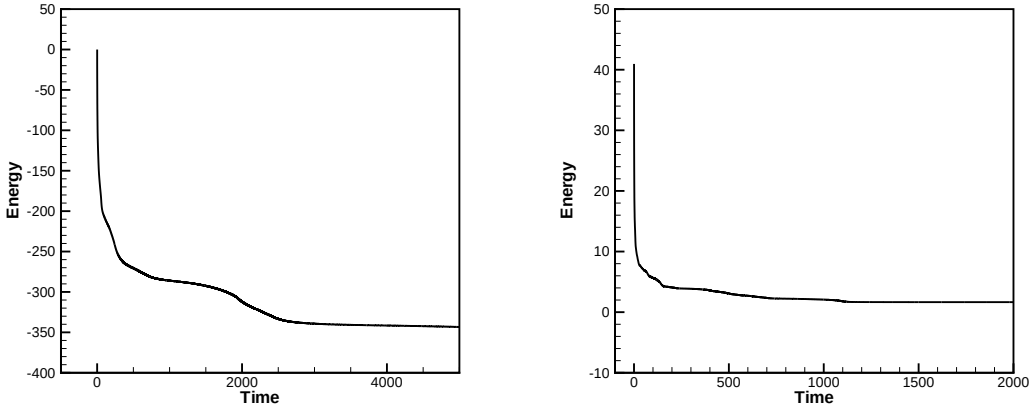

(a) MBE model without slope selection. (b) MBE model with slope selection.

Figure 10: Energy evolution of the SDC_2^2 method for the MBE models.

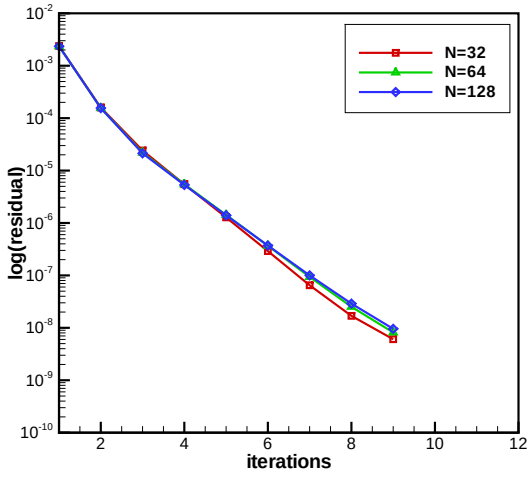

Figure 11: Convergence rates of multigrid solver with $\mathcal{P}^2$ approximation for the Cahn-Hilliard-Hele-Shaw system.

and the SDC$_3^3$ method for temporal discretization. The L^2 and L^∞ errors and the numerical orders of accuracy at time $T=0.5$ for the CHHS system is presented in Table 6, which shows the expected optimal $(r+1)$-th order of accuracy for $\mathcal{P}^r$ approximation. The convergence rates of the multigrid solver implemented with $\Delta t=0.001$ at the 10th time step is presented in Fig. 11, we can see the optimal complexity of the multigrid solver.

Table 6: Spatial and temporal accuracy test for the Cahn-Hilliard-Hele-Shaw system at time $T=0.5$. Here we choose the SDC$_3^3$ method with $\Delta t=0.1\Delta x$ and $\Delta x=2\pi/N$.

	N	L^2 error	order	L^∞ error	order
$\mathcal{P}^0$	16	2.16E-01	–	8.99E-02	–
	32	1.10E-01	0.97	4.63E-02	0.96
	64	5.55E-02	0.99	2.33E-02	0.99
$\mathcal{P}^1$	16	2.14E-02	–	1.50E-02	–
	32	5.34E-03	2.00	3.78E-03	1.99
	64	1.33E-03	2.00	9.45E-04	2.00
$\mathcal{P}^2$	16	1.43E-03	–	1.27E-03	–
	32	1.72E-04	3.06	1.56E-04	3.02
	64	2.16E-05	2.99	1.94E-05	3.01
$\mathcal{P}^3$	16	6.80E-05	–	8.69E-05	–
	32	4.26E-06	3.99	5.69E-06	3.93
	64	2.89E-07	3.88	3.98E-07	3.83

Topology changes. Here, we present an example to illustrate a topological change. We approximate the Cahn-Hilliard-Hele-Shaw system with $\varepsilon=0.1$ and $\gamma=4.0\varepsilon$ on a 128×128 grid for the computational domain $\Omega=[-4,4]\times[-4,4]$. We test the topological change with piecewise $\mathcal{P}^2$ approximations for spatial discretization and the SDC_2^2 method for temporal discretization with $\Delta t=0.1\Delta x$. The initial configuration consists of two almost touching surfaces-the inner surface being a circle and the outer surface being an ellipse. We can see a phenomenon of pinching off in Fig. 12. The energy evolution is presented in Fig. 13, where it is observed that the energy is non-increasing.

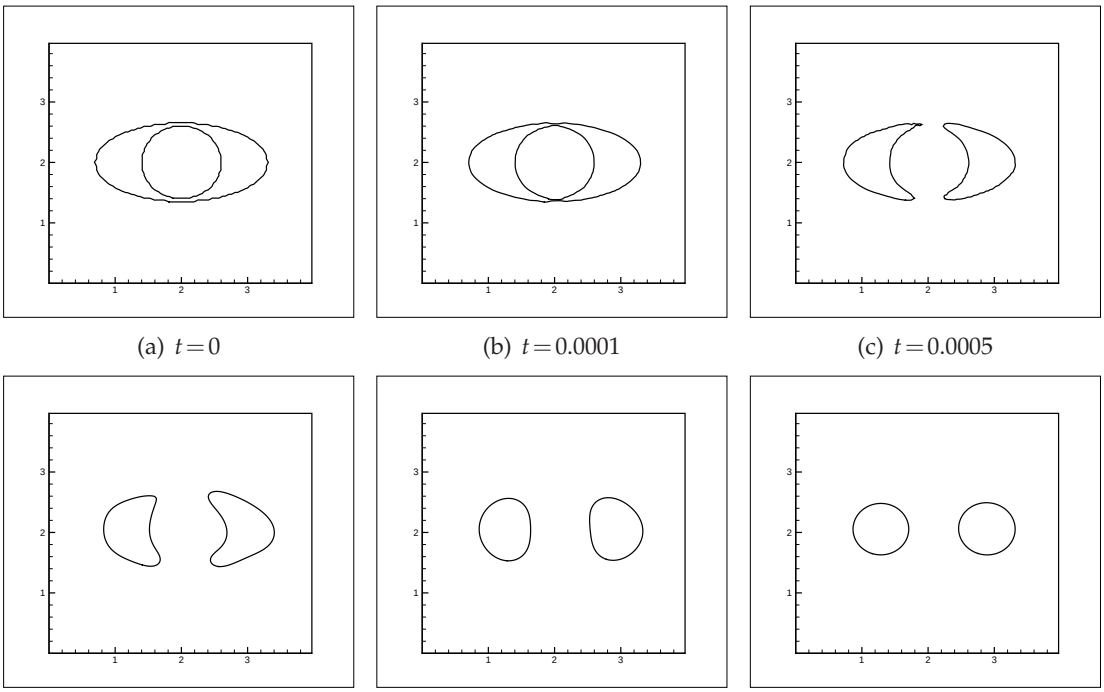

(a) $t=0$ (b) $t=0.0001$ (c) $t=0.0005$

(d) $t=0.01$ (e) $t=0.1$ (f) $t=0.5$

Figure 12: Topology changes. Two shapes pinch off under the evolution of the Cahn-Hilliard-Hele-Shaw system.

4 Concluding remarks

In this paper, we have developed a high order semi-implicit SDC method combining with energy stable linear schemes to approximate the Allen-Cahn equation, the Cahn-Hilliard equation, the molecular beam epitaxial growth models and the Cahn-Hilliard-Hele-Shaw system. The linear scheme is based on the invariant energy quadratization approach and it is proved to be unconditionally energy stable. For spatial discretization, we employ the local discontinuous Galerkin method. Combining with the semi-implicit SDC method, we can achieve high order accuracy in both time and space. Specially,

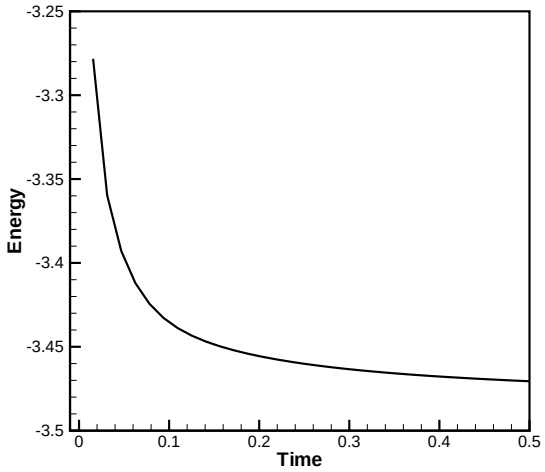

Figure 13: Energy evolution of the SDC_2^2 method with $\Delta t = 0.1\Delta x$ for the Cahn-Hilliard-Hele-Shaw system.

the linear scheme leads to linear algebraic equations to solve at each iteration, which can be solved efficiently by multigrid solver, namely, the multigrid solver has nearly optimal complexity. Numerical experiments are performed to verify that the proposed time marching methods are high order accurate and efficient when solving the phase field models.

Acknowledgments

Research of R. Guo is supported by NSFC grant No. 11601490. Research of Y. Xu is supported by NSFC grant No.11722112, 91630207.

Appendix A: LDG method for the Allen-Cahn equation

Before developing the LDG method, we first present some notations.

We consider a subdivision $\mathcal{T}_h$ of Ω with shape-regular elements K. Let $\mathcal{E}_h$ denote the union of the boundary faces of elements $K \in \mathcal{T}_h$, *i.e.* $\mathcal{E}_h = \bigcup_{K\in\mathcal{T}_h} \partial K$, and $\mathcal{E}_0 = \mathcal{E}_h \setminus \partial\Omega$. Let $\mathcal{P}^k(K)$ be the space of polynomials of degree at most $k \geq 0$ on $K \in \mathcal{T}_h$. The discontinuous Galerkin finite element spaces are denoted by

$$V_h = \Big\{ \varphi :\ \varphi|_K \in \mathcal{P}^k(K),\ \ \forall K \in \mathcal{T}_h \Big\},$$
$$\Sigma_h = \Big\{ \Phi = (\phi_1, \cdots, \phi_d)^T :\ \phi_l|_K \in \mathcal{P}^k(K),\, l = 1 \cdots d,\ \forall K \in \mathcal{T}_h \Big\}.$$

Notice that functions in V_h and Σ_h are allowed to be completely discontinuous across element interfaces.

In order to describe the flux functions, we need to introduce some notations. Let e be an interior face shared by the "left" and "right" elements K_L and K_R and define the normal vectors $\boldsymbol{\nu}_L$ and $\boldsymbol{\nu}_R$ on e pointing exterior to K_L and K_R, respectively. For our purpose, "left" and "right" can be uniquely defined for each face according to any fixed rule. For example, we choose $\boldsymbol{\nu}_0$ as a constant vector. The left element K_L to the face e requires that $\boldsymbol{\nu}_L\cdot\boldsymbol{\nu}_0<0$, and the right one K_R requires $\boldsymbol{\nu}_L\cdot\boldsymbol{\nu}_0\geq 0$. If ψ is a function on K_L and K_R, but possibly discontinuous across e, let ψ_L denote $(\psi|_{K_L})|_e$ and ψ_R denote $(\psi|_{K_R})|_e$, the left and right trace, respectively.

To develop the LDG scheme for (2.8)-(2.9), we first rewrite it as a first order system

$$\frac{\phi^{n+1}-\phi^n}{\Delta t}=b(\phi^n)p^{n+1}, \tag{A.1a}$$

$$p^{n+1}=\varepsilon^2\nabla\boldsymbol{q}^{n+1}-\phi^n U^{n+1}, \tag{A.1b}$$

$$\boldsymbol{q}^{n+1}=\nabla\phi^{n+1}, \tag{A.1c}$$

$$\frac{U^{n+1}-U^n}{\Delta t}=2\phi^n\frac{\phi^{n+1}-\phi^n}{\Delta t}. \tag{A.1d}$$

To simplify the notation, we still use ϕ^{n+1}, p^{n+1}, $\boldsymbol{q}^{n+1}$, U^{n+1} as the numerical solution. The LDG scheme to solve the system (A.1) becomes: Find ϕ^{n+1}, p^{n+1}, $U^{n+1}\in V_h$ and $\boldsymbol{q}^{n+1}\in\Sigma_h$, such that, for all test functions ξ, ζ, $\chi\in V_h$ and $\boldsymbol{\eta}\in\Sigma_h$, we have

$$\int_K\frac{\phi^{n+1}-\phi^n}{\Delta t}\xi dK=\int_K b(\phi^n)p^{n+1}\xi dK, \tag{A.2a}$$

$$\int_K p^{n+1}\zeta dK=-\int_K\varepsilon^2\boldsymbol{q}^{n+1}\cdot\nabla\zeta dK+\int_{\partial K}\widehat{\boldsymbol{q}}^{n+1}\cdot\boldsymbol{\nu}\zeta ds-\int_K\phi^n U^{n+1}\zeta dK, \tag{A.2b}$$

$$\int_K\boldsymbol{q}^{n+1}\cdot\boldsymbol{\eta}dK=-\int_K\phi^{n+1}\nabla\cdot\boldsymbol{\eta}dK+\int_{\partial K}\widehat{\phi}^{n+1}\boldsymbol{\eta}\cdot\boldsymbol{\nu}ds, \tag{A.2c}$$

$$\int_K\frac{U^{n+1}-U^n}{\Delta t}\chi dK=\int_K 2\phi^n\frac{\phi^{n+1}-\phi^n}{\Delta t}\chi dK. \tag{A.2d}$$

The "hat" terms in scheme (A.2) is the so-called "numerical fluxes", we can take the simple choices such as

$$\widehat{\phi}^{n+1}=\phi_R^{n+1},\quad \widehat{\boldsymbol{q}}^{n+1}=\boldsymbol{q}_L^{n+1} \tag{A.3}$$

to ensure the stability and local solvability of the intermediate variables.

Appendix B: The energy stability

Next, we will prove the energy stability for the fully-discrete LDG scheme (A.2) with the choice of the numerical fluxes (A.3).

Proposition B.1. (Energy stability for the first order linear LDG scheme) The solution to the LDG scheme (A.2) with the numerical fluxes (A.3) satisfies the energy stability

$$E_h(\boldsymbol{q}^{n+1},U^{n+1})-E_h(\boldsymbol{q}^n,U^n)\leq 0, \tag{B.1}$$

where

$$E_h(\boldsymbol{q},U)=\int_\Omega\left(\frac{1}{2}\varepsilon^2\boldsymbol{q}\cdot\boldsymbol{q}+\frac{1}{4}U^2\right)d\boldsymbol{x}.$$

Proof. For Eq. (A.2c) of the LDG scheme, subtracting the equations at time level t^n from the equation at time level t^{n+1}, and then taking the test function $\boldsymbol{\eta}=\boldsymbol{q}^{n+1}$, we get

$$\int_K(\boldsymbol{q}^{n+1}-\boldsymbol{q}^n)\cdot\boldsymbol{q}^{n+1}dK=-\int_K(\phi^{n+1}-\phi^n)\nabla\cdot\boldsymbol{q}^{n+1}dK+\int_{\partial K}(\widehat{\phi}^{n+1}-\widehat{\phi}^n)\boldsymbol{q}^{n+1}\cdot\boldsymbol{\nu}ds. \tag{B.2}$$

For other equations in scheme (A.2), we choose the test functions

$$\xi=-p^{n+1},\quad \zeta=\phi^{n+1}-\phi^n,\quad \chi=\frac{1}{2}U^{n+1},$$

respectively, to obtain

$$-\int_K\frac{\phi^{n+1}-\phi^n}{\Delta t}p^{n+1}dK=-\int_K b(\phi^n)p^{n+1}p^{n+1}dK, \tag{B.3}$$

$$\begin{aligned}\int_K p^{n+1}(\phi^{n+1}-\phi^n)dK=&-\int_K\varepsilon^2\boldsymbol{q}^{n+1}\cdot\nabla(\phi^{n+1}-\phi^n)dK+\int_{\partial K}\widehat{\boldsymbol{q}}^{n+1}\cdot\boldsymbol{\nu}(\phi^{n+1}-\phi^n)ds\\&-\int_K\phi^nU^{n+1}(\phi^{n+1}-\phi^n)dK,\end{aligned} \tag{B.4}$$

$$\int_K\frac{U^{n+1}-U^n}{2\Delta t}U^{n+1}dK=\int_K\phi^n\frac{\phi^{n+1}-\phi^n}{\Delta t}U^{n+1}dK. \tag{B.5}$$

Let $\frac{\varepsilon^2}{\Delta t}$(B.2)+(B.3)+$\frac{1}{\Delta t}$(B.4)+(B.5), with the help of the alternating numerical fluxes (A.3), and after a careful calculation, we obtain

$$\frac{\varepsilon^2}{\Delta t}\int_\Omega\boldsymbol{q}^{n+1}\cdot(\boldsymbol{q}^{n+1}-\boldsymbol{q}^n)d\boldsymbol{x}+\frac{1}{2\Delta t}\int_\Omega U^{n+1}(U^{n+1}-U^n)d\boldsymbol{x}+\int_\Omega b(\phi^n)(p^{n+1})^2d\boldsymbol{x}=0.$$

Using the identity

$$2(a-b,a)=|a|^2-|b|^2+|a-b|^2,$$

we can get the energy stability result (B.1) immediately. □

References

[1] J. Bosch, C. Kahle and M. Stoll, *Preconditioning of a Coupled Cahn-Hilliard Navier-Stokes System*, Commun. Comput. Phys., **23** (2018), pp.603-628.

[2] L. Chen, J. Zhao and X. Yang, *Regularized linear schemes for the molecular beam epitaxy model with slope selection*, Applied Numerical Mathematics, **128** (2018), pp.139-156.
[3] L.-Q. Chen, *Phase-field models for microstructural evolution*, Ann. Rev. Mater. Res., **32** (2002), pp.113-140.
[4] W.B. Chen, S. Conde, C. Wang, X. Wang and S. Wise, *A linear energy stable numerical scheme for epitaxial thin film growth model without slope selection*, J. Sci. Comput., **52** (2012), pp.546-562.
[5] B. Cockburn and C.-W. Shu, *TVB Runge-Kutta local projection discontinuous Galerkin finite element method for conservation laws II: general framework*, Math. Comp., **52** (1989), pp.411-435.
[6] B. Cockburn, S.-Y. Lin and C.-W. Shu, *TVB Runge-Kutta local projection discontinuous Galerkin finite element method for conservation laws III: one dimensional systems*, J. Comput. Phys., **84** (1989), pp.90-113.
[7] B. Cockburn, S. Hou and C.-W. Shu, *The Runge-Kutta local projection discontinuous Galerkin finite element method for conservation laws IV: the multidimensional case*, Math. Comp., **54** (1990), pp.545-581.
[8] B. Cockburn and C.-W. Shu, *The Runge-Kutta discontinuous Galerkin method for conservation laws V: multidimensional systems*, J. Comput. Phys., **141** (1998), pp.199-224.
[9] B. Cockburn and C.-W. Shu, *The local discontinuous Galerkin method for time-dependent convection-diffusion systems*, SIAM J. Numer. Anal., **35** (1998), pp.2440-2463.
[10] D.J. Eyre, *Unconditionally gradient stable time marching the Cahn-Hilliard equation*, in: J.W. Bullard, R. Kalia, M. Stoneham, L.Q. Chen (Eds.), Computational and Mathematical Models of Microstructural Evolution, vol.53, Materials Research Society, Warrendale, 1998, pp.1686-1712.
[11] X. Feng, T. Tang and J. Yang, *Long time numerical simulations for phase-field problems using p-adaptive spectral deferred correction methods*, SIAM J. Sci. Comput., **37** (2015), pp.A271-A294.
[12] R. Guo and Y. Xu, *Efficient solvers of discontinuous Galerkin discretization for the Cahn-Hilliard equations*, J. Sci. Comput., **58** (2014), pp.380-408.
[13] R. Guo, Y. Xia and Y. Xu, *An efficient fully-discrete local discontinuous Galerkin method for the Cahn-Hilliard-Hele-Shaw system*, J. Comput. Phys., **264** (2014), pp.23-40.
[14] R. Guo, L. Ji and Y. Xu, *High order local discontinuous Galerkin methods for the Allen-Cahn equation: analysis and simulation*, J. Comput. Math., **34** (2016), pp.135-158.
[15] R. Guo, Y. Xia and Y. Xu, *Semi-implicit spectral deferred correction methods for highly nonlinear partial differential equations*, J. Comput. Phys., **338** (2017), pp.269-284.
[16] J.S. Langer, *Models of pattern formation in first-order phase transitions*, Dir. in Cond. Matter Phys., World Sci. Pub. (1986), pp.164-186.
[17] D. Li and Z. Qiao, *On the stabilization size of semi-implicit Fourier-spectral methods for 3D Cahn-Hilliard equations*, Commun. Math. Sci., **15** (2017), pp.1489-1506.
[18] X. Li, Z. Qiao and H. Zhang, *An unconditionally energy stable finite difference scheme for a stochastic Cahn-Hilliard equation*, Sci. China Math., **59** (2016), pp.1815-1834.
[19] X. Li, Z. Qiao and H. Zhang, *A second-order convex splitting scheme for a Cahn-Hilliard equation with variable interfacial parameters*, J. Comput. Math., **35** (2017), pp.693-710.
[20] F. Liu and J. Shen, *Stabilized semi-implicit spectral deferred correction methods for Allen-Cahn and Cahn-Hilliard equations*, Math. Methods Appl. Sci., 2014.
[21] Z. Qiao, C. Wang and S.M. Wise, *Error analysis of a finite difference scheme for the epitaxial thin film model with slope selection with an improved convergence constant*, Int. J. Numer. Anal. Model., **14** (2017), pp.283-305.
[22] W. Reed and T. Hill, *Triangular mesh methods for the neutron transport equation*, Technical report LA-UR-73-479, Los Alamos Scientific Laboratory, Los Alamos, NM, 1973.

[23] J. Shen, C. Wang, X. Wang and S. Wise, *Second-order convex splitting schemes for gradient flows with Ehrlich-Schwoebel type energy: application to thin film epitaxy*, SIAM J. Numer. Anal., **50** (2012), pp.105-125.
[24] P. Song, T. Yang, Y. Ji, Z. Wang, L.Q. Chen and L. Chen, *A Comparison of Fourier Spectral Iterative Perturbation Method and Finite Element Method in Solving Phase-Field Equilibrium Equations*, Commun. Comput. Phys., **22** (2017), pp.1325-1349.
[25] T. Tang, W. Zhao, and T. Zhou, *Deferred Correction Methods for Forward Backward Stochastic Differential Equations*, Numer. Math. Theor. Meth. Appl., **10** (2017), pp.222-242.
[26] U. Trottenberg, C. Oosterlee and A. Schüller, *Multigrid*, Academic Press, New York (2005).
[27] S.M. Wise, *Unconditionally stable finite difference, nonlinear multigrid simulation of the Cahn-Hilliard-Hele-Shaw system of equations*, J. Sci. Comput., **44** (2010), pp.38-68.
[28] Y. Xia, *A fully discrete stable discontinuous Galerkin method for the thin film epitaxy problem without slope selection*, J. Comput. Phys., **280** (2015), pp.248-260.
[29] Y. Yan, W. Chen, C. Wang and S.M. Wise, *A Second-Order Energy Stable BDF Numerical Scheme for the Cahn-Hilliard Equation*, Commun. Comput. Phys., **23** (2018), pp.572-602.
[30] F. Yang, C. Venkataraman, V. Styles and A. Madzvamuse, *A Robust and Efficient Adaptive Multigrid Solver for the Optimal Control of Phase Field Formulations of Geometric Evolution Laws*, Commun. Comput. Phys., **21** (2017), pp.65-92.
[31] X. Yang, *Linear, first and second order and unconditionally energy stable numerical schemes for the phase field model of homopolymer blends*, J. Comput. Phys., **302** (2016), pp.509-523.
[32] X. Yang and D. Han, *Linearly first- and second-order, unconditionally energy stable schemes for the phase field crystal model*, J. Comput. Phys., **330** (2017), pp.1116-1134.
[33] X. Yang and L. Ju, *Efficient linear schemes with unconditionally energy stability for the phase field elastic bending energy model*, Comput. Methods Appl. Mech. Eng., **315** (2017), pp.691-712.
[34] X. Yang, J. Zhao and Q. Wang, *Numerical approximations for the molecular beam epitaxial growth model based on the invariant energy quadratization method*, J. Comput. Phys., **333** (2017), pp.104-127.
[35] X. Yang, J. Zhao, Q. Wang and J. Shen, *Numerical approximations for a three components Cahn-Hilliard phase-field model based on the invariant energy quadratization approach*, Math. Models Methods Appl. Sci., **27** (2017), pp.1993-2030.
[36] H. Yu and X. Yang, *Numerical approximations for a phase-field moving contact line model with variable densities and viscosities*, J. Comput. Phys., **334** (2017), pp.665-686.
[37] J. Zhao, Q. Wang and X. Yang, *Numerical approximations for a phase field dendritic crystal growth model based on the invariant energy quadratization approach*, Int. J. Numer. Methods Eng., **110** (2017), pp.279-300.
[38] J. Zhao, X. Yang, Y. Gong and Q. Wang, *A novel linear second order unconditionally energy stable scheme for a hydrodynamic Q-tensor model of liquid crystals*, Comput. Methods Appl. Mech. Engrg., **318** (2017), pp.803-825.
[39] Y. Zhang and W. Ye, *A Flux-Corrected Phase-Field Method for Surface Diffusion*, Commun. Comput. Phys., **22** (2017), pp.422-440.